An on-line testing technique for the scheduler memory of a GPGPU

On the principle of impedance-matching for underactuated wave energy harvesting systems

Nicolás Faedo[a,*], Fabio Carapellese[a], Edoardo Pasta[a], Giuliana Mattiazzo[a]

[a]*Marine Offshore Renewable Energy Lab., Department of Mechanical and Aerospace Engineering, Politecnico di Torino, 10129 Torino, Italy*

Abstract

In recent years, the fundamental principle of *impedance-matching* (IM) has inspired a number of sophisticated, yet *simple*, control solutions for wave energy converters (WEC). Such controllers have the capability of maximising energy absorption from incoming waves with mild computational requirements, being often intuitive in their design, hence especially appealing for real-time industrial applications. Nonetheless, these control solutions are, to date, almost exclusively developed for single degree-of-freedom (DoF) (and hence fully actuated) WEC systems, hindering their application to realistic *underactuated* multi-DoF devices, *i.e.* harvesting systems where energy is extracted from only a handful of its total set of modes of motion. Motivated by this, we present, in this paper, a comprehensive derivation and discussion of the IM conditions for maximum energy absorption in underactuated multi-DoF WEC systems. In particular, we show that the IM principle for single-DoF devices can be effectively extended to underactuated multi-DoF systems, and that a set of optimality conditions can be explicitly derived. In

*Corresponding author - E-mail: *nicolas.faedo@polito.it*

addition, we discuss both the impact and use of this set of optimal conditions for control design and synthesis, hence effectively taking a fundamental step towards the general extension of current IM-based techniques to the case of underactuated multi-DoF devices.

Keywords: Wave energy, WEC, energy-maximising control, optimal control, impedance-matching.

1. Introduction

Wave energy converters (WECs) inherently necessitate of appropriate control technology to guarantee maximum energy extraction from ocean waves: It is already well-established that efficient controllers can effectively reduce the levelised cost of wave energy, hence directly constituting a key stepping stone towards successful commercialisation of wide-spread WEC technology [1, 2].

The WEC control problem naturally falls under the umbrella of *optimal control theory*, where the control objective is, effectively, energy-maximisation from incoming waves. The associated WEC optimal control problem (OCP) has been solved using a variety of methods, most of which arise from the family of direct optimal control techniques (see, for instance, [3, 4]). Such strategies are essentially based upon discretising state and control variables involved in the corresponding OCP, to later attempt at maximising the resulting finite-dimensional nonlinear program (NP) directly, using numerical optimisation routines. The 'complexity' behind solving the associated NP depends upon a number of factors, being the specific discretisation tech-

nique considered to transcribe the OCP a primary driver (see *e.g.* [5, 6]). Relevant studies, which apply optimal control techniques to multiple degrees-of-freedom (DoFs) WEC systems (which constitute the main concern of this study), are, for instance, those presented in [7, 8, 9]. In particular, both [7] and [8] present a non-causal optimal controller, composed of a combination of feedback and feedforward structures, based upon the derivation in [10], while [9] presents a model predictive control (MPC) formulation[1].

Though controllers based on optimal control theory are effectively optimal by design, there is an increasing interest within the WEC control community in finding *simple* control solutions which do not rely upon potentially complex optimisation routines, which can preclude real-time application of OCP-based strategies. Such simple solutions are commonly referred to as *impedance-matching-based* (IM-based) controllers [11, 12], and are explicitly based on the fundamental theorem of maximum power transfer in electrical circuits: *i.e.* the *impedance-matching* (IM) principle [13]. In particular, this family of simple controllers attempts to provide a (physically implementable) realisation of the anti-causal impedance-matching condition for maximum power transfer, by proposing simple systems, *i.e.* using techniques arising from linear time-invariant (LTI) theory. As such, this family of controllers have mild computational requirements, and their implementation can be performed in real-time with almost any physical hardware platform. It is exactly this underlying simplicity what makes this set of strategies especially appealing for industrial applications, hence having the potential to become key

[1]The interested reader is referred to, for instance, [5], for a thorough discussion on MPC-based techniques in the WEC field.

enablers of advanced WEC technology. Examples of this class of controllers include [14, 15, 16, 17, 18, 19].

To date, IM-based controllers have virtually always been designed for single-DoF systems. While this could be sufficient in a handful settings, most wave energy systems present relevant dynamics in more than a single DoF [20, 21], rendering the application of current IM-based techniques potentially challenging. Furthermore, not only WECs are inherently multi-DoF, but naturally *underactuated*: Energy is often extracted from a single DoF, while the device effectively moves in multiple modes of motion (see *e.g.* [22, 23, 24]). This further complicates the direct application of current state-of-the-art IM-based techniques, hence directly hindering the potential application of this key family of simple controllers to realistic WEC systems. We do note, although, that the IM conditions for the idealised fully-actuated multi-DoF WEC case have been derived and discussed previously (see, for instance, [25, Chapter 6]), for the case of monochromatic (regular) wave inputs, *i.e.* in a narrowbanded sense, and applied to specific fully-actuated devices in, for example, [26], based upon the SISO structure [15].

The lack of IM-based techniques for this setting can be attributed to the absence of a general IM framework for underactuated multi-DoF harvesting systems: To the best of our knowledge, neither a formal discussion, nor a full derivation of the IM conditions for underactuated wave energy harvesters allowed to move in several modes of motions, *i.e.* underactuated multi-DoF WEC devices, has been presented in the literature of WEC control to date, hence precluding the natural extension of the single-DoF IM-based techniques to realistic and potentially complex WEC systems.

Motivated by the potential of this family of simple controllers to enable efficient WEC technology, we present, in this paper, a comprehensive derivation and discussion on the impedance-matching conditions for maximum energy absorption in underactuated multi-DoF WEC systems. In particular, we show that the IM principle for single-DoF devices can be effectively extended to underactuated multi-DoF systems, and that a set of optimality conditions can be explicitly derived. In addition, we discuss both the impact and use of this set of optimal conditions for control design and synthesis, making emphasis in typical IM-based control structures considered in the literature of single-DoF WECs, hence taking a fundamental step towards the general extension of current IM-based techniques to the case of underactuated multi-DoF devices. Among such design and synthesis conclusions, we show that the core design of optimal IM-based controllers *only depends upon the dynamics of the controlled DoFs*, and that any uncontrolled modes of motion can be 'left out' from the energy-maximising design, substantially simplifying the controller synthesis procedure.

The remainder of this paper is organised as follows. Section 1.1 introduces any non-standard notation utilised throughout our study. Section 2 recalls the well-known IM principle for single-DoF systems, making emphasis in the dynamical properties of the resulting optimal controller, and the associated optimality conditions. Section 3 derives and discusses the IM conditions for underactuated multi-DoF devices, while Section 4 considers such optimal energy-maximising conditions for control design and synthesis. Section 5 presents a case study to illustrate the results discussed in Sections 3 and 4. Finally, Section 6 encompasses the main conclusions of our manuscript.

1.1. Notation

Standard notation is used throughout our paper, with any exception detailed in this section. $\mathbb{R}^+$ ($\mathbb{R}^-$) denotes the set of non-negative (non-positive) real numbers. The symbol 0 stands for any zero element, dimensioned according to the context. The notation $\mathbb{N}_q$ indicates the set of all positive natural numbers up to q, *i.e.* $\mathbb{N}_q = \{1, 2, \ldots, q\}$. The symbol $\mathbb{I}_n$ denotes the identity matrix of the space $\mathbb{C}^{n\times n}$. The *real-* and *imaginary-part* of a complex matrix $z \in \mathbb{C}^{n\times n}$ are denoted as $\Re(z)$ and $\Im(z)$, respectively. The Laplace transform of a function f (provided it exists), is denoted as $F(s)$, $s \in \mathbb{C}$. The Hermitian operator is denoted by $F^\star(\jmath\omega)$, where $\omega \in \mathbb{R}$. With some abuse of notation, the same notation is used for the analytic continuation of the Hermitian operator to the Laplace domain, *i.e.* the *parahermitian* conjugate [27], which is defined as $F^\star(s) = F(-s)^\intercal$, for $s \in \mathbb{C}$. In addition, we denote the Hermitian-inverse composition $F^{-1\star} = F^{\star-1}$ simply as $F^{-\star}$.

2. The IM principle for single DoF devices

As briefly discussed in Section 1, one of the first and fundamental results applied within the wave energy control literature relies on approaching the energy-maximising problem in terms of the theory of impedance-matching for electrical circuits. We recall and discuss the application of this principle for single-DoF wave energy systems in the following paragraphs, adopting a system dynamics perspective. The interested reader is referred to, for instance, [28] and [25, Chapter 6], for further detail on the topics recalled in this section.

Consider a WEC device represented in terms of a LTI operator $G : \mathbb{C} \to$

$\mathbb{C}$, $s \mapsto G(s)$, affected by the superposition of two distinctive inputs: an external uncontrollable force $f : \mathbb{R}^+ \to \mathbb{R}$, $t \mapsto f(t)$, *i.e.* the so-called *wave excitation force*, and a user-supplied *control* action $u : \mathbb{R}^+ \to \mathbb{R}$, $t \mapsto u(t)$, *i.e.* the power take-off (PTO) force. To be precise, the output of the WEC, commonly defined to be the associated velocity corresponding with the single mode of motion of the device, *i.e.* $v : \mathbb{R}^+ \to \mathbb{R}$, $t \mapsto v(t)$, can be computed in terms of the following Laplace-domain relation,

$$V(s) = G(s)\left[F(s) - U(s)\right], \tag{1}$$

where the existence of each associated Laplace transform is inherently guaranteed from the physical properties of the energy harvesting process (see, for instance, [11, 29]).

Remark 1. The derivation of the operator G from physical principles is standard in the literature of WEC control, and hence it is not discussed in this section for the sake of brevity. The reader is referred to, for instance, [29, 30, 31], for a thorough treatment on this topic. We do list, although, the fundamental dynamical properties of G, which are relevant in the derivation of the IM for wave energy systems:

- $\diamond$ The mapping G is input-output stable.
- $\diamond$ $G(s)$ is strictly proper.
- $\diamond$ $G(s)$ is minimum-phase.
- $\diamond$ $G(s)$ is positive-real.

Based upon the relation expressed in (1), we now recall the IM principle for WEC systems. Let $I : \mathbb{C} \to \mathbb{C}$, $\jmath\omega \mapsto I(\jmath\omega)$, be the so-called WEC

intrinsic impedance, defined in terms of the frequency-response of system G such as

$$I(\jmath\omega) = \frac{1}{G(\jmath\omega)}, \tag{2}$$

so that the input-output frequency-response of the associated WEC system (1) can be expressed in terms of I as

$$V(\jmath\omega) = \frac{1}{I(\jmath\omega)} \left[F(\jmath\omega) - U(\jmath\omega) \right]. \tag{3}$$

Equation 3 naturally resembles well-known representations in the field of electrical/electronic engineering and circuits theory. In particular, setting $U = I_u V$, where I_u is commonly referred to as the *control load*, the WEC relation (3) is of an output feedback type, and can be equivalently described by an analogue circuit, as depicted in Figure 1.

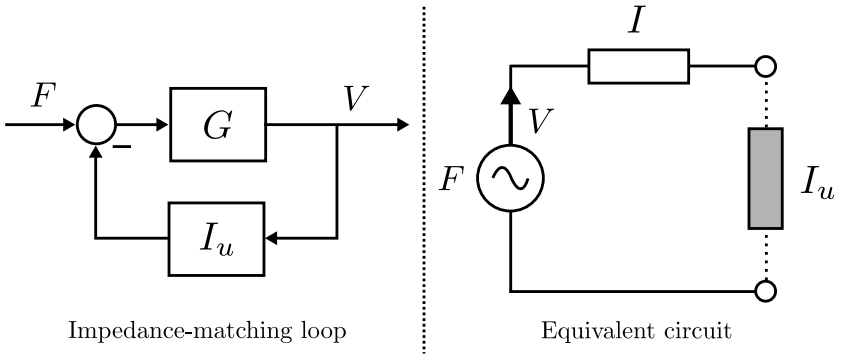

Figure 1: Impedance-matching feedback control loop for single-DoF WEC systems (left), and its equivalent circuit representation (right).

From the perspective offered in Figure 1, the control force, defined in terms of the load I_u, has to be designed by the user so that maximum power transfer is achieved from the source, *i.e.* the wave excitation force F.

This problem can be directly addressed using the well-established *impedance-matching* (or *maximum power transfer*) theorem [13]: the load impedance, I_u, should be designed such that it exactly coincides with the complex-conjugate of the intrinsic (WEC) impedance, I. To be precise, the control load is to be designed such that the following frequency-domain condition,

$$I_u(\jmath\omega) = I^\star(\jmath\omega) = \frac{1}{G^\star(\jmath\omega)}. \tag{4}$$

holds, (ideally) for all $\omega \in \mathbb{R}$, *i.e.* in a broadband sense. The optimal selection of I_u in (4) renders a specific optimal closed-loop mapping T^{opt}, which can be fully written in terms of G as,

$$T^{\text{opt}}(\jmath\omega) = \frac{G(\jmath\omega)G^\star(\jmath\omega)}{G(\jmath\omega) + G^\star(\jmath\omega)} = \frac{\Re(G(\jmath\omega))^2 + \Im(G(\jmath\omega))^2}{2\Re(G(\jmath\omega))}, \tag{5}$$

where note that $T^{\text{opt}}(\jmath\omega) \in \mathbb{R}^+$, *i.e.* T^{opt} is an *ideal filter* (see, for instance, [32]) and hence has *zero phase*. The fact that the image of T^{opt} belongs to the set of positive real numbers is a direct consequence of the positive-real nature[2] of G (see Remark 1).

The very nature of the condition expressed in (5) has been widely used within the WEC control literature, since it expresses a fundamental condition for maximum energy absorption in this single-DoF device case: *Under optimal energy absorption conditions, the output velocity v of the WEC system is a scaled version of the wave excitation force input f.* We can split this last statement into two well-known conditions:

Phase condition: The instantaneous phase of the velocity v under optimal control conditions is synchronised with that of the excitation input f.

[2]The reader is referred to [28, 29] for further discussion on this topic.

Amplitude condition: The instantaneous amplitude of the velocity v under optimal control conditions is that of the excitation force f, scaled by the mapping T^{opt}.

Going further with the analysis of the key elements behind this IM approach for single-DoF devices, note that, if we consider the analytic continuation of I_u to all of $\mathbb{C}$, we can define the optimal control law, *i.e.* u such that condition (5) holds, simply as

$$U(s) = \frac{1}{G^{\star}(s)} V(s) = K(s)V(s), \tag{6}$$

where, clearly, (6) is of an output (velocity) feedback nature, as per illustrated in Figure 1.

Remark 2. One fundamental conclusion can be directly drawn from the relation (6) and the set of properties for G listed in Remark 1: Given the nature of G, the optimal controller K in (6) is stable but *anti-causal*, *i.e.* it fully requires *future* input information to achieve optimal energy-absorption [25]. In other words, K as in (6) cannot be physically implemented, which is precisely what leads researchers to attempt at achieving causal controllers which approximate the control law presented in (6), *i.e.* to propose *impedance-matching-based* solutions (see also the discussion provided in Section 1).

Though the optimality conditions expressed throughout this section effectively represent a powerful tool for control design and synthesis, these only comprise the case of a single-DoF (and hence fully actuated) WEC device. This automatically precludes the natural extension of IM-based solutions to more realistic cases, where the WEC system is assumed to be multi-DoF and underactuated.

3. IM for underactuated multi-DoF devices

As discussed throughout Section 1, the main objective of this paper is to provide a formal derivation and discussion on the set of optimality conditions, arising from the principle of impedance-matching, for multi-DoF WEC systems. We recall that, in general, this type of systems are *underactuated*, since energy absorption is virtually always harvested from a single mode of motion, *i.e.* the control force acts over a single DoF (see *e.g.* [33, 23]). Exceptions to this rule also exists, and we can find devices, such as [34, 35], which extract energy in more than one operation mode. Nonetheless, either in the former or the latter cases, WEC systems are naturally underactuated, and we virtually always have 'less' control inputs than the total number of modes of motion associated to any device. We provide a precise treatment of the associated IM optimality conditions in the following paragraphs.

Remark 3. As briefly discussed in Section 1, the theory for maximum energy-absorption for fully actuated multi-DoF systems has been previously derived and discussed in, for instance, [25, Chapter 6]. In particular, [25, Chapter 6] discusses the IM-principle under two main assumptions: Firstly, the input wave excitation is considered to be composed of a single frequency component (*i.e.* regular), and hence the analytical analysis provided is simplified by operating on the so-called *complex amplitude* associated to each variable involved in the derivation of the optimal velocity profile. Secondly, the velocity profile for each DoF is considered to be freely assignable, which directly translates, in a controlled scenario, to a fully actuated device. While this scenario effectively provides the maximum theoretical power that can be achieved in these idealised conditions, effective absorption (*i.e.* converted

power/energy) virtually always occur in a finite number of DoFs (from the total modes of motion of the WEC) in practical applications (as discussed in the paragraph immediately above this remark), situation which the theory presented in [25, Chapter 6] does not cover. This is, indeed, exactly what motivates the discussion presented in the following paragraphs, which provide a formal derivation of the broadband IM-conditions for underactuated multi-DoF devices.

3.1. Multi-DoF devices with a single control input

To begin our exposition, we consider a WEC system with $N \in \mathbb{N}$ DoFs, defined in terms of an LTI operator G (analogously to the single-DoF case presented in Section 2). Suppose each DoF is affected by an external uncontrollable wave excitation force input f_i, with $i \in \mathbb{N}_N$, but that energy is extracted *only in a single mode of motion*, which is controlled via a user-supplied law u. This is, indeed, the most likely scenario (in a physical sense), and only one PTO system is commonly available to extract energy from a specific mode of motion. Finally, without any loss of generality, let v_1 be the output velocity associated to the controlled DoF. The equation of motion of such a WEC can be written in the Laplace-domain analogously to (1), in

particular[3]:

$$V_1 = \begin{bmatrix} G_1 & G_2 & \dots & G_N \end{bmatrix} \begin{bmatrix} F_1 - U \\ F_2 \\ \vdots \\ F_N \end{bmatrix}, \tag{7}$$

where $G_i(s) \in \mathbb{C}$ represents the mapping from the i-th input to the controlled output v_1.

Remark 4. The mapping G_1, *i.e.* the transfer function characterising the map $f_1 - u_1 \mapsto v_1$, has the exact same list of properties as those listed in Section 2 for the single-DoF case. Furthermore, each element in the set $\{G_i\}_{i=2}^N$ is input-output stable. The interested reader is referred to, for instance, [29, 36], for further detail.

In view of the results we aim to present in this section, we first note that equation (7) can be conveniently re-written as

$$V_1 = G_1 \left[\tilde{F}_1 - U \right], \tag{8}$$

where the mapping $\tilde{F}_1$, defined as

$$\tilde{F}_1 = F_1 + \sum_{i=2}^{N} \frac{G_i}{G_1} F_i, \tag{9}$$

is the *total* wave excitation force acting on the controlled DoF.

Remark 5. The mapping $\tilde{F}_1$ is the result of superimposing the wave excitation force acting on the controlled DoF, f_1, with the 'contribution' of the wave

[3]From now on, we drop the dependence on s when clear from the context, for simplicity of exposition.

excitation forces acting on the other $N-1$ modes of motion. Note that such contributions are effectively modulated by a corresponding *stable* transfer function, *i.e.* G_i/G_1, $i \in \mathbb{N}_N \backslash \{1\}$. The stability of G_i/G_1, for all admissible i, follows trivially from the minimum-phase property of G_1 (see Remark 4).

Given the nature of the expression derived in (8)-(9), we can consider an analogous approach to IM to that described in Section 2 for single-DoF devices. In particular, let us define the intrinsic impedance of the underactuated multi-DoF WEC (8) as

$$I = \frac{1}{G_1}, \tag{10}$$

so that the associated control-loop can be seen as a analog circuit, with source $\tilde{F}$ (*i.e.* total wave excitation force), as schematically depicted in Figure 2. The optimal energy-maximising control force can be then directly computed in terms of the parahermitian conjugate of G_1, *i.e.*

$$U = I_u V_1 = \frac{1}{G_1^\star} V_1, \tag{11}$$

and, hence, the optimal closed-loop input-output response T^{opt}, characterising the map $\tilde{F}_1 \mapsto V_1$ under controlled conditions, is given by

$$T^{\text{opt}} = \frac{G_1 G_1^\star}{G_1 + G_1^\star}, \tag{12}$$

where, since G_1 shares the properties listed in Remark 1, it is straighforward to check that $T^{\text{opt}} : \mathbb{C} \to \mathbb{R}^+$, *i.e.* T^{opt} is an ideal zero-phase filter. Though 'similar' to the IM condition for single-DoF systems, the case derived in this section possesses a number of fundamental differences, particularly with respect to the associated set of (phase and amplitude) optimality conditions.

Before discussing such optimal behaviour, we note that, due to the linerity of WEC model, the response of the harvester under optimal controlled conditions can be written in terms of the following expansion:

$$V_1 = T^{\text{opt}} F_1 + \sum_{i=2}^{N} \frac{G_i}{G_1} T^{\text{opt}} F_i = V_1^1 + \sum_{i=2}^{N} V_1^i, \tag{13}$$

where $V_1^1 = T^{\text{opt}} F_1$ and $V_1^i = (G_i/G_1) T^{\text{opt}} F_i$, *i.e.* in terms of the contribution of each exciting force f_i, $i \in \mathbb{N}_N$, in the optimally controlled output v_1. We now proceed to detail the corresponding optimal phase and amplitude conditions for this underactuated multi-DoF WEC case. **Phase conditions:**

- ◇ The instantaneous phase of the velocity of the controlled DoF v_1 under optimal control conditions is synchronised with that of the *total* excitation input $\tilde{f}$.

- ◇ The instantaneous phase of v_1^1 under optimal control conditions is synchronised with that of the excitation input acting on the same DoF, *i.e.* f_1.

- ◇ The instantaneous phase of v_1^j, $j \in \mathbb{N}_N \backslash \{1\}$, under optimal control conditions, and the wave excitation force corresponding to the j-th DoF, *i.e.* f_j, have an optimal phase difference given by $\underline{/G_j/G_1}$.

Amplitude conditions:

- ◇ The instantaneous amplitude of the velocity of the controlled DoF v_1 under optimal control conditions is that of the *total* excitation force $\tilde{f}$, scaled by the mapping T^{opt} in (12).

◇ The instantaneous amplitude of v_1^1 under optimal control conditions is that of the excitation input acting on the same DoF, f_1, scaled by the mapping T^{opt} in (12).

◇ The instantaneous amplitude of v_1^j, $j \in \mathbb{N}_N \backslash \{1\}$, under optimal control conditions is that of the wave excitation force corresponding to the j-th DoF, f_j, scaled by the mapping $|G_j/G_1|T^{\text{opt}}$, with T^{opt} as in (12).

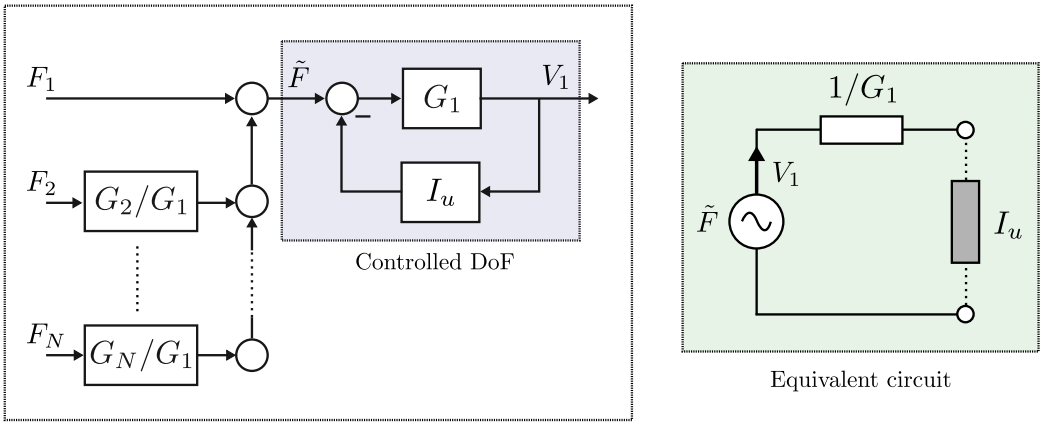

Figure 2: Impedance-matching feedback control-loop for multi-DoF devices with a single controlled DoF (left), and its equivalent circuit representation (right).

The conditions stated in the paragraph immediately above resemble those described for the single-DoF device case, in Section 2, with a number of fundamental differences. In particular, the 'in-phase' condition with the external excitation is somewhat preserved in the following sense: The optimal output velocity is effectively synchronised with the *total* excitation force acting on the actuated DoF. Furthermore, in the absence of all wave excitation forces but that acting on the specific controlled DoF, *i.e.* $f_i = 0$, $i \in \mathbb{N}_N \backslash \{1\}$, the phase synchronisation property is still inherited from the single-DoF IM

theory. This can be directly appreciated from Figure 2, where it is clear that f_1 has a 'direct-path' (*i.e.* a path with unitary gain) to the closed-loop controlled DoF. In turn, the optimal phase with respect to any other excitation force (from that acting directly on the controlled DoF), is fully determined by the phase of G_j/G_1, *i.e.* $\angle G_j/G_1$.

A similar set of conclusions can be drawn for the case of the amplitude conditions, where the existence of an optimal scaling mapping T^{opt} is also inherently present in this underactuated multi-DoF case. In particular, the optimal controlled velocity v_1 is indeed a 'scaled version' of the total wave excitation force $\tilde{f}_1$ acting on the actuated DoF, *i.e.* $V_1 = T^{\text{opt}}\tilde{F}_1$. Same behavior can be appreciated if only $f_1 \neq 0$, $\forall t$, consistent with the single-DoF IM theory of Section 2. In turn, the optimal transfer from any other excitation force (from that acting directly on the controlled DoF), is scaled to the output via the composite mapping $|G_j/G_1|T^{\text{opt}}$.

Remark 6. The optimality conditions derived and discussed in this section have a strong impact on practical control design considerations for underactuated multi-DoF devices, being able to greatly simplify optimal control synthesis for potentially complex WEC systems. We provide a detailed discussion of such considerations, in Section 4.

3.2. Multi-DoF devices with multiple control inputs

We now consider the more general case, *i.e.* a WEC system with $N \in \mathbb{N}$ DoFs, defined in terms of an LTI operator G, where each DoF is affected by an external uncontrollable wave excitation force input f_i, with $i \in \mathbb{N}_N$, but, differently from the case discussed in Section 3.1, energy is now extracted in

the first $1 < m < N$ modes of motion. Note that the system is, effectively, underactuated, being u_i, with $i \in \mathbb{N}_m$, each associated control input.

Let each output (velocity) associated to the first m (controlled) DoFs be denoted as v_i, with $i \in \mathbb{N}_m$. Analogously to (1) and (7), the equation of motion of such a WEC can be compactly written in the Laplace-domain as

$$V_u = \begin{bmatrix} G_u & G_{\bar{u}} \end{bmatrix} \begin{bmatrix} F_u - U \\ F_{\bar{u}} \end{bmatrix}, \tag{14}$$

where $G_u(s) \in \mathbb{C}^{m\times m}$, $G_{\bar{u}} \in \mathbb{C}^{m\times(N-m)}$, $\{F_u(s), U(s), V_u(s)\} \subset \mathbb{C}^m$, and $F_{\bar{u}} \in \mathbb{C}^{(N-m)}$, are defined as

$$\begin{aligned} G_u &= \begin{bmatrix} G_{11} & \dots & G_{1m} \\ \vdots & \ddots & \vdots \\ G_{m1} & \dots & G_{mm} \end{bmatrix}, \quad G_{\bar{u}} = \begin{bmatrix} G_{1(m+1)} & \dots & G_{1N} \\ \vdots & \ddots & \vdots \\ G_{m(m+1)} & \dots & G_{mN} \end{bmatrix}, \\ F_u &= \begin{bmatrix} F_1 \\ \vdots \\ F_m \end{bmatrix}, F_{\bar{u}} = \begin{bmatrix} F_{m+1} \\ \vdots \\ F_N \end{bmatrix}, U = \begin{bmatrix} U_1 \\ \vdots \\ U_m \end{bmatrix}, V_u = \begin{bmatrix} V_1 \\ \vdots \\ V_m \end{bmatrix}. \end{aligned} \tag{15}$$

Remark 7. The mappings G_u and $G_{\bar{u}}$ in (15) describe the dynamics associated to controlled and uncontrolled DoFs, respectively. Note that, while G_u maps both wave excitation forces and control inputs associated with the first m controlled nodes, $G_{\bar{u}}$ specifies the contribution of the wave excitation forces acting on the $N - m$ uncontrolled DoFs in the set of controlled outputs, *i.e.* the entries of V_u.

Remark 8. Note that G_u inherits the very same properties described in Remark 1 for the single-DoF case, now with the corresponding multiple-input

multiple-output (MIMO) definitions (see also [37, 36]).

Analogously to the case presented in (8), equation (14) can be conveniently re-expressed as

$$V_u = G_u \left[\tilde{F}_u - U \right], \tag{16}$$

where the mapping $\tilde{F}_u$ is defined as

$$\tilde{F}_u = F_u + G_u^{-1} G_{\bar{u}} F_{\bar{u}}. \tag{17}$$

Remark 9. As in the case of (9), equation (17) describes (in a compact form) the *total* wave excitation acting on the set of controlled DoFs, being directly composed of the sum of two contributions: The excitation force acting on the first m nodes, F_u, and the effect of the wave excitation affecting the uncontrolled modes, $F_{\bar{u}}$, mapped by the (stable) corresponding transfer function $G_u^{-1} G_{\bar{u}}$.

By defining the intrinsic impedance of the underactuated multi-DoF WEC (16) as

$$I = G_u^{-1}, \tag{18}$$

the optimal energy-maximising control force (vector) U can be computed analogously to Section 3.1, *i.e.* in terms of the parahermitian conjugate of G_u, *i.e.*

$$U = I_u V_u = G_u^{-\star} V_u. \tag{19}$$

Finally, the corresponding optimal closed-loop input-output response T^{opt}, characterising the mapping $\tilde{F}_u \mapsto V_u$ under controlled conditions, can be then computed as

$$T^{\text{opt}} = \left(\mathbb{I}_m + G_u G_u^{-\star} \right)^{-1} G_u = G_u^{\star} \left(G_u^{\star} + G_u \right)^{-1} G_u. \tag{20}$$

While the properties associated with (20) for the general case are, in principle, not trivial to assess (given its inherent MIMO nature), we perform the following 'simplification', which is fully motivated by the physical nature of the associated mapping G_u. In particular, given the inherent symmetry in the dynamical interactions between different modes of motion (see, for instance, [37]), the frequency-response associated to G_u is virtually always characterised in terms of a symmetric operator, *i.e.* $G_u(\jmath\omega) = G_u(\jmath\omega)^\intercal$. Suppose such property holds and, without any loss of generality, let the frequency-response of G_u be decomposed as $G_u(\jmath\omega) = X_u(\omega) + \jmath Y_u(\omega)$, where $X_u(\omega) = \Re(G_u(\jmath\omega))$ and $Y_u(\omega) = \Im(G_u(\jmath\omega))$. Noting that, under the assumed symmetry, $G_u^\star(\jmath\omega) = X(\omega) - \jmath Y(\omega)$, the frequency-response associated with the optimally controlled closed-loop (20) can be expressed as

$$T^{\text{opt}}(\jmath\omega) = \frac{1}{2}\left(X(\omega) + Y(\omega)X(\omega)^{-1}Y(\omega)\right), \tag{21}$$

i.e. $T^{\text{opt}}(\jmath\omega) \in \mathbb{R}^{m\times m}$, and hence T^{opt} in (20) is also an ideal zero-phase filter.

Remark 10. If $m = N = 1$, the symmetry of G_u holds trivially, and it is straightforward to check that condition (21) coincides with the well-known optimal frequency-response expressed in (5) for single-DoF WEC systems.

Remark 11. In the limit case $m = N$, *i.e.* where we can effectively control every DoF of the device via a specific control input, the result of (21) (and the associated optimal control input in (19)), coincide with the theory presented in [25, Chapter 6], for fully actuated multi-DoF WEC devices.

We note that, having derived the corresponding optimal closed-loop response (20)-(21), the phase and amplitude conditions for the case presented in this

section can be obtained analogously to those presented in Section 3.1, and hence we avoid a detailed discussion for economy of space.

4. Controller design and synthesis

We dedicate this section to the analysis of the impact of the optimality conditions derived in Section 3 on control design and synthesis for underactuated WEC systems. In particular, we make special emphasis in how the fundamental ideas behind so-called IM-based controllers, originally developed for single-DoF devices, can be directly translated to synthesise implementable LTI controllers for the underactuated multi-DoF WEC case, based upon the results of Section 3. We note that, throughout this section, we adopt the WEC representation (and associated notation) utilised in Section 3.2.

Recall that IM-based controllers aim to approximate the energy-maximising IM conditions, which are inherently non-causal, and hence require future information of either the incoming wave description (in a feedforward control configuration), or the corresponding device motion (in a feedback structure). Such an approximation is commonly perfomed, in the literature of single-DoF devices, via *causal* and *stable* LTI systems, providing *simple* control solutions which can be implemented in real-time straightforwardly[4]. Such techniques employ *three* very distinctive control configurations, schematically illustrated in Figure 3, which we herein generalise to the underactuated multi-DoF WEC

[4]There is, naturally, a loss of performance when approximating the non-causal IM conditions by a causal LTI system. Though this is beyond the scope of this study, which aims at extending the IM conditions for underactuated devices, and analyse its use in control applications, the reader is referred to *e.g.* [11] for further discussion on this topic.

case.

Remark 12. Though beyond the scope of this paper, we note that many of the conclusions elucidated within this section can be also translated to the family of optimal-control-based WEC controllers, where techniques from optimal control theory are directly used to solve for the energy-maximising control law.

A first fundamental feature, which can be directly extracted from the derivation and discussion presented in Section 3, is that, independently of the specific control structure selected, the optimal energy-maximising design and synthesis process *depends only upon the dynamics associated with the controlled DoFs*, *i.e.* G_u. In other words, the dynamics associated with the uncontrolled DoFs, $G_{\bar{u}}$, can be, in principle, 'disregarded' within the design and synthesis of the corresponding IM-based controller. We do note, although, that the dynamics described by $G_{\bar{u}}$ play a role in the design of any state constraint handling mechanism, since the actual motion under controlled conditions is indeed affected by $G_u^{-1}G_{\bar{u}}$.

4.1. Controller structure ***(a)***

The control structure **(a)**, defined in Figure 3, is of a feedback nature: Output measurements are used directly in a feedback configuration, together with a typically dynamic *stable and causal* (*i.e.* implementable) controller K_{fb}. This feedback controller is to be designed such that it approximates the corresponding IM condition for maximum energy absorption. Examples of this type of controllers, developed for single-DoF devices, are [17, 16].

Note that, clearly, 'true' optimality cannot be achieved in this setting, since the associated optimal impedance $I_u = G_u^{-\star}$ is given in terms of the

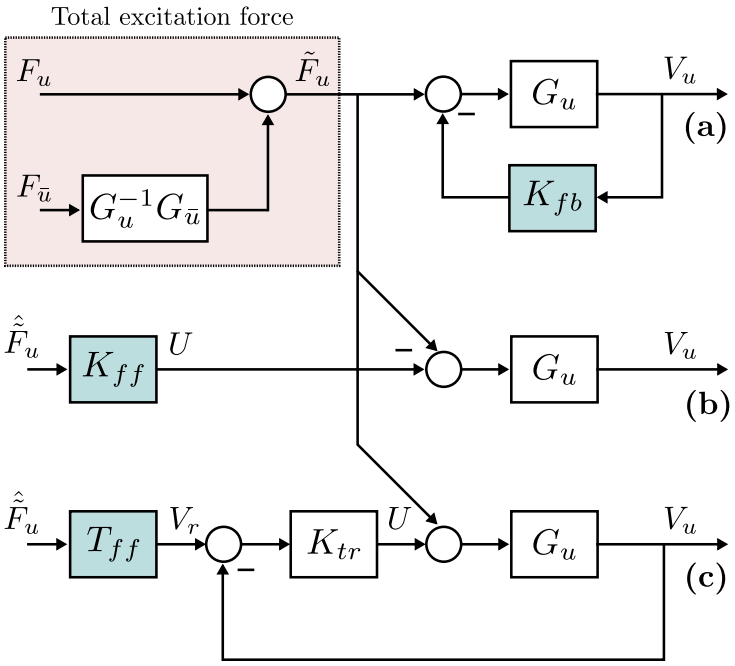

Figure 3: Typical IM-based control configurations adapted for underactuated multi-DoF systems.

inverse of the parahermitic conjugate of G_u, which is inherently *anti-causal*. Following the derivation provided in Section 3, we hence define K_{fb} such that the approximate broadband condition

$$\|K_{fb}(\jmath\omega) - I_u(\jmath\omega)\|_2 \approx 0, \quad \omega \in \mathcal{W}, \tag{22}$$

holds, where the set $\mathcal{W} \subset \mathbb{R}$ denotes a range of frequencies of interest. Such a set is directly motivated by the 'operational space' of the specific controlled device, *i.e.* the stochastic nature of the wave excitation.

Remark 13. It is worth highlighting that, even if K_{fb}, accomplishing (22), is designed to be stable and causal (properties which are relatively simple to achieve with standard model reduction/system identification techniques),

there is no guarantee, in general, of a stable closed-loop response. In other words, an additional condition (constraint) should be added to (22) in order to guarantee a well-posed closed-loop.

A typical design that fits the control structure discussed in this section, which is widely considered within the WEC community for single-DoF devices, is the so-called "reactive controller", which is essentially a feedback structure achieving the IM condition for a single (input) frequency $\omega_p \in \mathbb{R}$. To date, in the literature of underactuated multi-DoF devices, such a controller is often found via exhaustive search (see *e.g.* [33, 38]), which can be time consuming and, in general, lacks of convergence guarantees. Following the derivation of the IM conditions presented in this paper, in Section 3, such a controller can be simply designed by fulfilling the interpolation condition:

$$K_{fb}(\jmath\omega_p) = I_u(\jmath\omega_p), \tag{23}$$

hence directly avoiding any numerical optimisation routines. A specific example case on how to use this interpolation condition is offered in Section 5.

4.2. Controller structure ***(b)***

In contrast to the feedback structure described in Section 4.1, the control loop **(b)**, defined in Figure 3, is of a feedforward nature. This specific structure comes with one fundamental advantage: the stability of the control loop can be directly guaranteed by forcing the structure K_{ff} to be stable (and causal, for implementability). The main disadvantage is such a feedforward configuration inherently requires knowledge of the wave excitation, which is not measurable in practice [39, 40]. An example of this control strategy can be found in, for instance, [18].

We begin this section by unveiling a fundamental consequence of the results discussed in Section 3, for feedforward-based structures, such as **(b)** and **(c)** in Figure 3. In particular, the current WEC control literature, adopting this specific type of structure, commonly estimates the 'full' wave excitation force vector $[F_u^\intercal \ F_{\bar{u}}^\intercal]^\intercal$ to implement the optimal control force, *i.e.* an estimation of the N wave excitation forces acting on both controlled and uncontrolled modes of motion is computed to provide an optimal energy-absorption PTO law. Nonteheless, a fundamental result, which can be directly extracted from Section 3, is that *only an estimation of the total wave excitation $\tilde{F}_u$ acting on the controlled DoFs is required to implement such a control structure.* In other words, only $m < N$ forces need to be estimated to achieve optimality. Note that this key conclusion directly extends to optimal-control-based strategies, which are virtually always composed of an optimal feedforward path [12]. From now on, we denote the estimation of the total wave force as $\hat{\tilde{F}}_u$.

Remark 14. For most WEC prototypes developed in the literature, only a single DoF is controlled, *i.e.* the case discussed in Section 3.1, so that the estimation of a *single external force is sufficient to optimal achieve energy-maximisation.* This (single) approximation can be obtained using well-established single-input single-output (SISO) unknown-input estimation techniques, such as those extensively described in [39].

With respect to the design of K_{ff} to achieve optimal energy-absorption for underactuated devices, we note that the optimal condition in this setting can be directly derived from equation (20). In particular, if we assume that $\hat{\tilde{F}}_u = \tilde{F}_u$, the associated optimal input-output mapping can be trivially ex-

pressed as $T^{\text{opt}} = (\mathbb{I}_m - I_{u_{ff}})G_u$, where the 'feedforward-control-impedance', $I_{u_{ff}}$, can be simply defined as,

$$I_{u_{ff}} = \mathbb{I}_m - G_u^{\star}(\mathbb{I}_m + G_u G_u^{-\star})^{-1}. \tag{24}$$

Similarly as in the feedback case discussed in Section 4.1, the causal and stable controller K_{ff} is selected such that the approximate broadband conditions

$$\|K_{ff}(\jmath\omega) - I_{u_{ff}}(\jmath\omega)\|_2 \approx 0, \quad \omega \in \mathcal{W}, \tag{25}$$

holds, with $\mathcal{W}$ a set of relevant frequencies.

4.3. Controller structure ***(c)***

The last control structure discussed, *i.e.* the control loop **(c)** in Figure 3, relies upon the generation of an optimal velocity reference profile, V_r, in terms of an approximation of the optimal closed-loop response given by a causal and stable mapping T_{ff}. This structure is then of a feedforward type, as the case of **(b)**, but where the optimal input-output response T^{opt} is approximated directly. In addition, a tracking controller K_{tr} is introduced, aiming to achieve asymptotic tracking of the generated optimal reference V_r. Note that we leave K_{tr} out of the following discussion, since such a controller can be synthesised based upon a plethora of standard techniques arising both from classical, and modern control theory. Examples of controller adopting the feedforward structure **(c)**, for single-DoF WECs, are [15, 19].

Remark 15. As per the case discussed in Section 4.3, it is sufficient to provide an estimate of the total wave excitation force acting on the controlled DoFs, *i.e.* $\hat{\tilde{F}}_u$, to implement the feedforward structure **(c)**.

The mapping T_{ff} can be then designed analogously to K_{fb} and K_{ff} in Sections 4.1 and 4.3, respectively. In particular, T_{ff} is to be synthesised such as the approximate broadband condition

$$\|T_{ff}(\jmath\omega) - T^{\mathrm{opt}}(\jmath\omega)\|_2 \approx 0, \quad \omega \in \mathcal{W}, \tag{26}$$

holds, where, if $G_u(\jmath\omega) = G_u(\jmath\omega)^\intercal$, the ideal frequency-response $T^{\mathrm{opt}}(\jmath\omega)$ is as defined in (21).

5. Case study

With the objective of providing an explicit illustration of the IM conditions for multi-DoF underactutated WEC systems, derived in Section 3, and elucidate how these can be used in the design of IM-based controllers, we present, in this section, a case study[5] considering a WEC geometry inspired by [24], and illustrated herein in Figure 4. The associated dimensions and quantities defining such a WEC are presented in Table 1. The device is considered to be allowed to move in two different DoFs, *pitch* and *surge*, but has a single PTO sitting on the *pitch axis only*, *i.e.* is underactuated. Such a DoF is kept aligned with the corresponding input wave direction. Note that the set of optimality conditions for this device corresponds with the theory of Section 3.1. The corresponding hydrodynamic parameters have been computed using the open-source boundary element method (BEM) solver [41].

[5]Given the main objective of this section, we note that any comparison with existing control techniques is beyond the scope of our study. Nonetheless, we do refer the reader to, for instance, [12], for a comparison study between IM-based control solutions, and non-causal optimal-control-based techniques for wave energy systems.

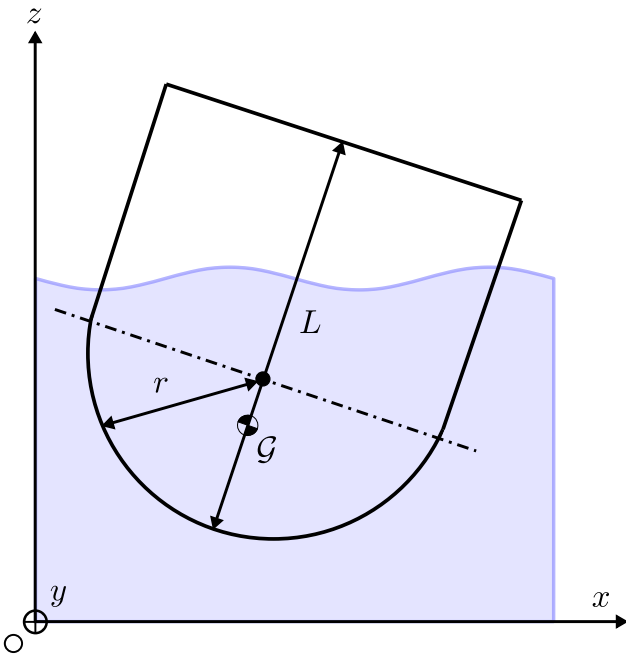

Figure 4: Schematic illustration of the considered WEC geometry.

Characteristic	**Value**
Length (L)	14.8 [m]
Radius (r)	7.4 [m]
Depth	21.18 [m]
Mass	1298 [ton]
Pitch moment of inertia	4.62 [kg m^2]
Center of gravity ($\mathcal{G}$)	1.19 [m]

Table 1: Relevant parameters for the considered WEC device.

In particular, let v_1 denote the output velocity corresponding with pitch motion, so that the WEC under study can be represented in terms of an LTI mapping $G = [G_1\ G_2]$, as per the case of equation (7), with G_1 representing the (inner) dynamics characterising the controlled DoF, and G_2 describing the 'impact' of surge motion in the pitch dynamics. The frequency-response mappings associated with $\{G_1, G_2\}$ are represented, for the absorber depicted

in Figure 4, in the Bode plot of Figure 5. Note that, as per derived in Section 3, the optimal impedance depends only upon G_1.

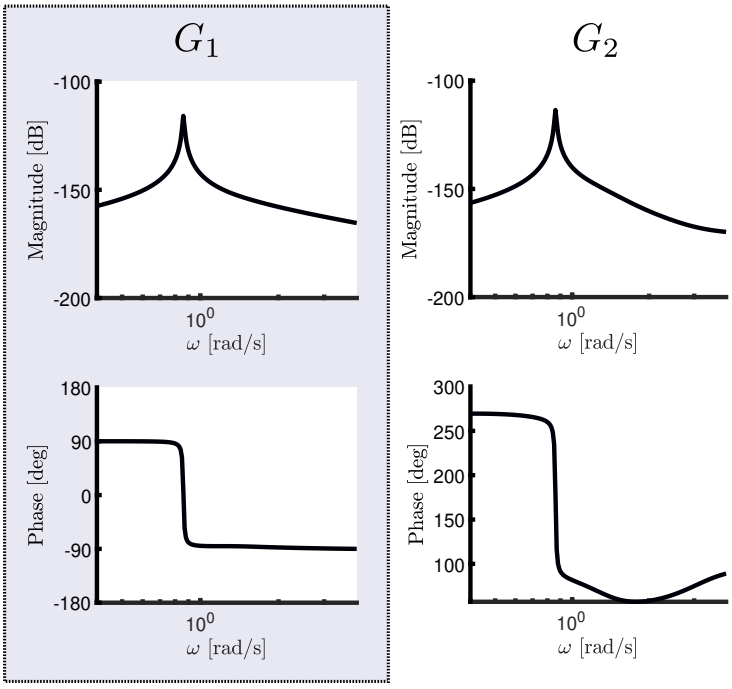

Figure 5: Bode plot associated with the dynamics $G = [G_1\ G_2]$ of the considered WEC device.

Figure 6 (left) illustrates the frequency-response associated with two key mappings: The optimal transfer function characterising $\tilde{f}_1 \mapsto v_1$, *i.e.* the optimal closed-loop dynamics relating the total wave excitation force and corresponding output velocity, and that of the mapping G_2/G_1, which relates the wave excitation force acting in surge with the pitch velocity v_1. Note that, as expected from the discussion provided in Section 3, T^{opt} is an ideal zero-phase filter. Though the optimality conditions presented in Figure 6 are indeed fully broadband, *i.e.* valid for any $\omega \in \mathbb{R}$, Figure 6 (right) also

provides a (steady-state) time-domain analysis of such energy-maximising behaviour for a specific input frequency. In particular, we consider that both f_1 and f_2 arise from a monochromatic (regular) wave input, with a period of $T_0 = 6.5$ [s], and a height of $H_0 = 2$ [m]. Note that the corresponding input frequency is $\omega_0 = 2\pi/T_0 \approx 0.98$ [rad/s].

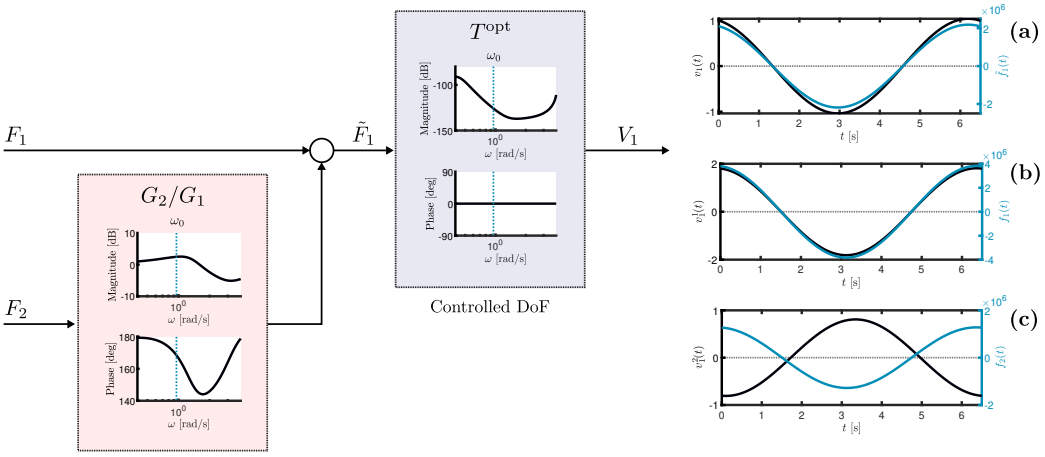

Figure 6: Frequency-domain impedance-matching conditions for the underactuated WEC (left), along with a time-domain analysis for a specific input frequency $\omega \approx 0.98$ [rad/s] (right - **a**, **b** and **c**).

Figure 6 **(a)** directly shows the 'in-phase' behaviour between the total wave excitation force $\tilde{f}_1$, and pitch velocity v_1, under optimally controlled conditions, consistently with the derivation of Section 3. The same phenomena can be noted in Figure 6 **(b)**, between the wave excitation force acting on pitch, *i.e.* f_1, and the corresponding 'component' in the output velocity v_1^1, as expected from equation (13). Finally, a shift of approximately 170° can be appreciated in Figure 6 **(c)**, between the excitation acting on surge f_2, and its corresponding contribution in the pitch velocity v_1^2. Note that, clearly, such a phase difference coincides with the phase of G_1/G_2 at the

specific input frequency ω_0. An analogous set of conclusions can be drawn for the amplitude conditions discussed in Section 3.1, for all **(a)**, **(b)**, and **(c)** cases.

Although the primary objective of this section is to illustrate the optimality conditions derived in Section 3, we offer herein a brief example on how to apply the controller synthesis ideas exposed in Section 4. In particular, given its ubiquitous nature within the WEC control literature, we use the IM conditions to design a reactive controller for the considered underactuated WEC of Figure 4, in terms of a proportional-integral (PI) structure, *i.e.* we design a stable output feedback controller

$$K_{fb}(s) = \theta_1 + \frac{\theta_2}{s}, \tag{27}$$

where $\{\theta_1, \theta_2\} \subset \mathbb{R}$ are selected to interpolate the optimal anti-causal control impedance I_u, defined via equation (11), at a specific input frequency. Consistent with the discussion provided in Section 4, the selection of such an interpolation point is herein motivated by the nature of the WEC operating conditions. For instance, we assume in the following that the pitching absorber is subject to a stochastic sea-state, fully characterised in terms of a spectral density function with a peak wave period of $T_p = 6.5$ [s]. Such a peak period corresponds with a peak frequency $\omega_p = \omega_0 \approx 0.98$ [rad/s].

After setting the interpolation point to be the peak frequency $\jmath\omega_p$, it is straightforward to show that the following selection for the parameters in (27)

$$\theta_1 = \Re(I_u(\jmath\omega_p)), \quad \theta_2 = -\omega_p \Im(I_u(\jmath\omega_p)), \tag{28}$$

are such that $K_{fb}(\jmath\omega_p) = I_u(\jmath\omega_p)$. For the specific WEC considered, $\theta_1 \approx 1.05 \times 10^6$ and $\theta_2 \approx 1.02 \times 10^7$.

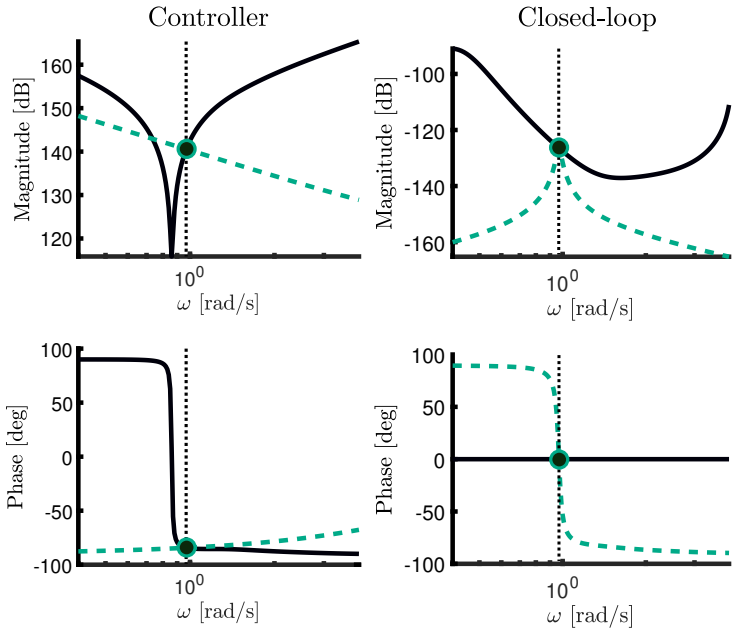

Figure 7: Optimal controller (left-solid) and closed-loop responses (right-solid), along with the corresponding feedback PI controller (left-dashed) and closed-loop response (right-dashed), achieving interpolation at ≈ 0.98 [rad/s].

The Bode plot presented in Figure 7 (left) explicitly illustrates the frequency-response of the optimal impedance I_u of the WEC under study (solid), along with the frequency-response associated with the reactive PI controller K_{fb} of (27), with parameters tuned following (28) (dashed). It can be readily appreciated that K_{fb} effectively interpolates the optimal controller response I_u at the peak frequency characterising the sea-state. Furthermore, the Bode plot of Figure 7 (right) shows the optimal (ideal-filter) closed-loop response T^{opt} for the considered WEC (solid), and that obtained with the reactive PI controller (dashed), where, naturally, the interpolation at ω_p can be directly appreciated, meaning that K_{fb} effectively approximates the optimal input-output response in a neighbourhood of the interpolation frequency selected.

6. Conclusions

Motivated by the key benefits of IM-based control techniques for single-DoF devices, we present, in this paper, a detailed derivation and discussion of the impedance-matching principle for the (more general and realistic) case of underactuated multi-DoF devices. In particular, we elucidate the full set of optimality conditions for such a case, and unveil its impact on control design and synthesis of IM-based controllers for potentially complex WEC systems, making explicit emphasis in the extension of well-known control structures to the case of underactuated multi-DoF devices. We illustrate the proposed results in terms of a case study, where the set of optimal conditions is explicitly shown in both the frequency- and time-domains, together with the design of an implementable feedback (interpolating) structure. The set of optimality conditions, and associated impact on different control structures, presented in our study, represents a key stepping stone towards the development of novel IM-based controllers for realistic WEC systems, hence contributing in the path towards effectively enabling advanced WEC technology.

ACKNOWLEDGMENT

This project has received funding from the European Union's Horizon 2020 research and innovation programme under the Marie Sklodowska-Curie grant agreement No 101024372. The results of this publication reflect only the author's view and the European Commission is not responsible for any use that may be made of the information it contains

References

[1] J. Ringwood, G. Bacelli, F. Fusco, Energy-maximizing control of wave-energy converters: The development of control system technology to optimize their operation, IEEE Control Systems 34 (5) (2014) 30–55.

[2] K. Ruehl, D. Bull, Wave Energy Development Roadmap: Design to commercialization, OCEANS 2012 MTS/IEEE: Harnessing the Power of the Ocean (2012).

[3] D. Liberzon, Calculus of Variations and Optimal Control Theory: A Concise Introduction, Princeton University Press, 2011.

[4] F. Fahroo, I. M. Ross, Pseudospectral methods for infinite-horizon nonlinear optimal control problems, Journal of Guidance, Control, and Dynamics 31 (4) (2008) 927–936.

[5] N. Faedo, S. Olaya, J. V. Ringwood, Optimal control, mpc and mpc-like algorithms for wave energy systems: An overview, IFAC Journal of Systems and Control 1 (2017) 37–56.

[6] N. Faedo, G. Scarciotti, A. Astolfi, J. V. Ringwood, Nonlinear energy-maximizing optimal control of wave energy systems: A moment-based approach, IEEE Transactions on Control Systems Technology (Early access) (2021).

[7] Z. Liao, P. Stansby, G. Li, E. C. Moreno, High-capacity wave energy conversion by multi-floats, multi-pto, control and prediction: generalised

state-space modelling with linear optimal control and arbitrary headings, IEEE Transactions on Sustainable Energy (Early access available) (2021).

[8] Z. Liao, P. Stansby, G. Li, A generic linear non-causal optimal control framework integrated with wave excitation force prediction for multi-mode wave energy converters with application to m4, Applied Ocean Research 97 (2020) 102056.

[9] A. Hillis, J. Yardley, A. Plummer, A. Brask, Model predictive control of a multi-degree-of-freedom wave energy converter with model mismatch and prediction errors, Ocean Engineering 212 (2020) 107724.

[10] S. Zhan, G. Li, Linear optimal noncausal control of wave energy converters, IEEE Transactions on Control Systems Technology 27 (4) (2018) 1526–1536.

[11] D. García-Violini, N. Faedo, F. Jaramillo-Lopez, J. V. Ringwood, Simple controllers for wave energy devices compared, Journal of Marine Science and Engineering 8 (10) (2020) 793.

[12] N. Faedo, D. García-Violini, Y. Peña-Sanchez, J. V. Ringwood, Optimisation-vs. non-optimisation-based energy-maximising control for wave energy converters: A case study, in: European Control Conference (ECC), IEEE, 2020, pp. 843–848.

[13] R. L. Thomas, A practical introduction to impedance matching, Artech House, 1976.

[14] F. Fusco, J. V. Ringwood, et al., Suboptimal causal reactive control of wave energy converters using a second order system model, in: Proceedings of the 21st International Offshore and Polar Engineering (ISOPE) Conference, Maui, International Society of Offshore and Polar Engineers, 2011, pp. 687–694.

[15] F. Fusco, J. V. Ringwood, A simple and effective real-time controller for wave energy converters, IEEE Trans. Sustain. Energy 4 (2013) 21–30.

[16] J. Song, O. Abdelkhalik, R. Robinett, G. Bacelli, D. Wilson, U. Korde, Multi-resonant feedback control of heave wave energy converters, Ocean Engineering 127 (2016) 269–278.

[17] G. Bacelli, V. Nevarez, R. G. Coe, D. G. Wilson, Feedback resonating control for a wave energy converter, IEEE Transactions on Industry Applications 56 (2) (2019) 1862–1868.

[18] D. García-Violini, Y. Peña-Sanchez, N. Faedo, J. V. Ringwood, An energy-maximising linear time invariant controller (lite-con) for wave energy devices, IEEE Transactions on Sustainable Energy 11 (4) (2020) 2713–2721.

[19] P. B. Garcia-Rosa, G. Kulia, J. V. Ringwood, M. Molinas, Real-time passive control of wave energy converters using the hilbert-huang transform, IFAC-PapersOnLine 50 (1) (2017) 14705–14710.

[20] G. Giorgi, J. V. Ringwood, A compact 6-dof nonlinear wave energy device model for power assessment and control investigations, IEEE Transactions on Sustainable Energy 10 (1) (2018) 119–126.

[21] G. Giorgi, R. P. Gomes, J. C. Henriques, L. M. Gato, G. Bracco, G. Mattiazzo, Detecting parametric resonance in a floating oscillating water column device for wave energy conversion: Numerical simulations and validation with physical model tests, Applied Energy 276 (2020) 115421.

[22] G. Bracco, M. Canale, V. Cerone, Optimizing energy production of an inertial sea wave energy converter via model predictive control, Control Engineering Practice 96 (2020) 104299.

[23] J. H. Todalshaug, G. S. Ásgeirsson, E. Hjálmarsson, J. Maillet, P. Möller, P. Pires, M. Guérinel, M. Lopes, Tank testing of an inherently phase-controlled wave energy converter, International Journal of Marine Energy 15 (2016) 68–84.

[24] N. Pozzi, G. Bracco, B. Passione, S. A. Sirigu, G. Mattiazzo, Pewec: Experimental validation of wave to pto numerical model, Ocean Engineering 167 (2018) 114–129.

[25] J. Falnes, Ocean Waves and Oscillating Systems: Linear Interactions Including Wave-Energy Extraction, Cambridge University Press, 2002.

[26] A. Hillis, C. Whitlam, A. Brask, J. Chapman, A. Plummer, Active control for multi-degree-of-freedom wave energy converters with load limiting, Renewable Energy 159 (2020) 1177–1187.

[27] P. Fuhrmann, Elements of factorization theory from a polynomial point of view, in: Three decades of mathematical system theory, Springer, 1989, pp. 148–178.

[28] J. Scruggs, On the causal power generation limit for a vibratory energy harvester in broadband stochastic response, Journal of Intelligent Material Systems and Structures 21 (13) (2010) 1249–1262.

[29] R. Taghipour, T. Perez, T. Moan, Hybrid frequency–time domain models for dynamic response analysis of marine structures, Ocean Engineering 35 (7) (2008) 685–705.

[30] J. Falnes, A. Kurniawan, Ocean Waves And Oscillating Systems: Linear Interactions Including Wave-Energy Extraction, Vol. 8, Cambridge University Press, 2020.

[31] N. Faedo, Y. Peña-Sanchez, J. V. Ringwood, Finite-order hydrodynamic model determination for wave energy applications using moment-matching, Ocean Engineering 163 (2018) 251–263.

[32] L. D. Paarmann, Design and analysis of analog filters: a signal processing perspective, Vol. 617, Springer Science & Business Media, 2006.

[33] S. A. Sirigu, G. Vissio, G. Bracco, E. Giorcelli, B. Passione, M. Raffero, G. Mattiazzo, Iswec design tool, International Journal of Marine Energy 15 (2016) 201–213.

[34] L. Wang, J. V. Ringwood, Control-informed ballast and geometric optimisation of a three-body hinge-barge wave energy converter using two-layer optimisation, Renewable Energy 171 (2021) 1159–1170.

[35] F. Paparella, J. V. Ringwood, Optimal control of a three-body hinge-barge wave energy device using pseudospectral methods, IEEE Transactions on Sustainable Energy 8 (1) (2017) 200–207.

[36] T. Pérez, T. I. Fossen, Time-vs. frequency-domain identification of parametric radiation force models for marine structures at zero speed, Modeling, Identification and Control 29 (1) (2008) 1–19.

[37] M. Folley, D. Forehand, Chapter 8 - conventional multiple degree-of-freedom array models, in: M. Folley (Ed.), Numerical Modelling of Wave Energy Converters, Academic Press, 2016, pp. 151 – 164.

[38] M. Raffero, M. Martini, B. Passione, G. Mattiazzo, E. Giorcelli, G. Bracco, Stochastic control of inertial sea wave energy converter, The Scientific World Journal 2015 (2015) ID–980613.

[39] Y. Peña-Sanchez, C. Windt, J. Davidson, J. V. Ringwood, A critical comparison of excitation force estimators for wave-energy devices, IEEE Transactions on Control Systems Technology 28 (6) (2020) 2263–2275.

[40] N. Faedo, Y. Peña-Sanchez, J. V. Ringwood, Parametric representation of arrays of wave energy converters for motion simulation and unknown input estimation: a moment-based approach, Applied Ocean Research 98 (2020) 102055.

[41] A. Babarit, G. Delhommeau, Theoretical and numerical aspects of the open source BEM solver NEMOH, in: 11th European Wave and Tidal Energy Conference, Nantes, 2015.